

# Optimal Controller Gain for the Control Based Continuation of a Duffing-Oscillator

Gleb Kleyma, Sebastian Tatzko, Jörg Wallaschek

*Institute of Dynamics and Vibration Research, Leibniz University Hannover, Germany*

*Summary.* In the context of control based continuation for the experimental identification of nonlinear dynamic systems a PD-controller is usually exploited to stabilize the unstable branches of so called S-curves. The literature often refers to a simple trial-and-error method in order to determine the controller gains. In this paper the optimal controller gains for a Duffing-oscillator are determined analytically by applying the Harmonic Balance Method (HBM) to obtain a nonlinear algebraic approximation. However, the generalized methodology can be easily extended to any kind of nonlinear dynamic system.

## Introduction

Experimental or Control-Based Continuation (CBC) is a promising method for the bifurcation analysis in real life nonlinear experiments. Exploiting the CBC method, it is possible to track a branch of periodic solutions through a fold bifurcation where they become unstable and continue them up to a second bifurcation point where they become stable again. A typical example for such behavior is the frequency response of vibrating structures featuring nonlinear stiffness, [1]. Typically, thin structures tend to behave like this, as they become geometrically nonlinear when excited to vibration amplitudes in the order of their thickness. In particular, it can be shown that the nonlinear restoring force of thin shell elements can be described by quadratic and cubic stiffness terms, [2, 3]. Considering a modal approach, in the more specific case of a transversely loaded hinged-hinged beam, a Duffing-type differential equation can be assumed, [4]. Here, the stiffness term is cubic, but depends on the mode-shape and type of support.

Experimental characterization of nonlinear oscillating systems is a challenging task. There are only few methods that will identify a nonparametric model of the structure, [5]. CBC is one of these methods. The goal of CBC is to estimate the nonlinear frequency response curves (NLFR). Originally, CBC was proposed by [6] as a tool for the bifurcation analysis of a dry-friction oscillator. However, since then the application of CBC has already been experimentally demonstrated on various systems, such as a parameter excited pendulum [7], an electromagnetic and piezoelectric energy harvesting device [8, 9, 10], a nonlinear tuned mass damper (NTMD) [11], a beam with a locally attached nonlinear spring [12], an impact oscillator [13], a Duffing-oscillator, and frictionally coupled beams [14]. There are also several publications that deal with different extensions and improvements compared to the original method. For instance, the adaption of CBC for tracking of backbone-curves [15, 16], increased robustness against measurement noise [17] and the application of FIR-filters to speed up the measurement time [18]. Even the stability of periodic orbits can be assessed during a CBC experiment, as described in [11] and [19].

A main concern in CBC is the applied control strategy. A feedback control is essential to stabilize the unstable periodic orbits of the system in order to trace them through the bifurcation points. Typically, a PD-controller, corresponding to figure 2 is exploited. After finding suitable controller gains, the amplitude  $\hat{x}_{\text{ref}}$  of the reference signal is swept (or stepped) and the corresponding force is measured. By means of Newtons method (full CBC), fixed point iteration or an adaptive FIR-filter (simplified CBC), the controller is constrained to be stabilizing but non-invasive with respect to the system dynamics. For the determination of the controller gains, literature often refers to a trial-and-error procedure. However, this can be very time-consuming if at least approximate values are unforeseen. Besides the trial-and-error procedure, in [20], stability maps were created for an impact oscillator by varying the controller gains and evaluating the resulting control error. In that way the optimal settings for this specific experiment were found. Unfortunately, these findings can not be generalized for different types of systems. An application of adaptive control strategies to CBC was presented in [21]. Although the authors approach is formulated for linear systems, they have showed that the method can be successfully applied to nonlinear examples as well. However, the mathematical derivation of the controller equation is very challenging and a generalized proof of concept for nonlinear systems is still pending. This is why we feel like the major control problem is not yet fully solved.

This paper deals with an analytical approximate solution of critical controller gains for a Duffing-type oscillator in a CBC experiment. The Harmonic Balance Method is applied on the closed-loop system in order to determine stabilizing gains of the PD-controller. The results are validated on an experimental single-degree-of-freedom nonlinear oscillator. The concept can be adapted to other systems including the initially mentioned geometrically nonlinear structures. With the developed formula one is capable of predicting the critical controller gains, which can be considered as lower limits, where stabilization is granted. It will be shown, that for polynomial nonlinearities only the polynomial degree and not the coefficients are essential. This makes it very easy to estimate the necessary structural parameters.

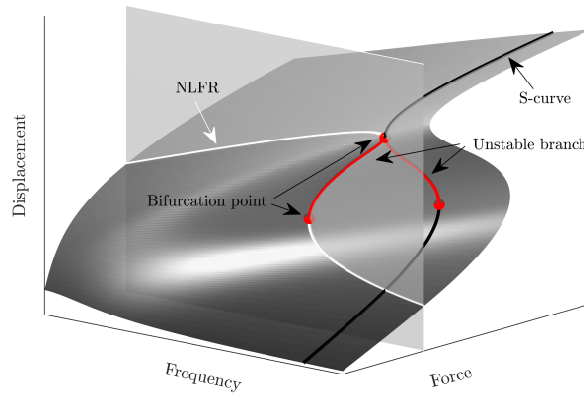


Figure 1: Manifold of a single degree of freedom Duffing-oscillator. White: Nonlinear frequency response curve (NLFR), Black: S-curve, Red lines: Unstable branches, Red dots: Fold bifurcation

Figure 1 shows the displacement amplitude of a stiffening Duffing-oscillator as a three-dimensional manifold plotted versus the excitation frequency and excitation force. The white curve is the nonlinear frequency response (NLFR) of the system. The red dots mark bifurcation points and the red curves are unstable periodic solutions. The black curve can be interpreted as the load-displacement characteristic of the system at a constant excitation frequency. Due to the particular shape, it is referred to as a S-curve in literature. Both types of curves (NLFRs and S-curves) are projections of the same manifold to different parameter spaces. Accordingly, an experimental characterization of such systems can be performed in two different ways: A continuation of the NLFRs varying two parameters at a time (frequency and displacement) like proposed by [20] (full CBC) or tracing the S-curves at constant frequency (simplified CBC). Due to the unique correlation between displacement and forcing amplitude in many systems, the latter approach can be considered as the simpler method. The continuation parameter reduces then to a single variable, which is the displacement amplitude. Either way (full or simplified CBC) a feedback controller is essential to stabilize the unstable periodic orbits.

We will focus on the simplified CBC in this paper. Here, each frequency corresponds to a measurement run and so the control parameters can be adjusted between the runs, if necessary. For a detailed description of the CBC method, please refer to the previously mentioned literature. An application of CBC to the experimental Duffing-oscillator presented within this paper is also found in [14].

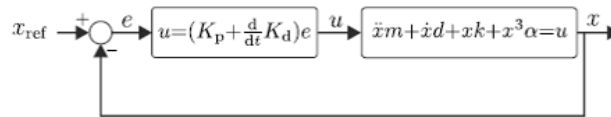


Figure 2: Feedback control loop utilized for control-based continuation.

### Condition for a Stabilizing Controller

The equation of motion (EOM) of the forced Duffing-oscillator reads:

$$m\ddot{x} + d\dot{x} + kx + \alpha x^3 = f. \quad (1)$$

Here  $f$  is the excitation force and  $x$  is the displacement. Harmonically excited at certain frequencies, in open-loop condition, the system features two stable and one unstable periodic solution, as shown in figure 1. The goal is to stabilize the system by a feedback controller such that for a given reference displacement  $x_{\text{ref}}$  the unstable branch is accessible. A simple PD-controller, corresponding to figure 2, is exploited for this purpose. In closed-loop the excitation force can be expressed in terms of the controller gains ( $K_p$ ,  $K_d$ ) and displacements ( $x$ ,  $x_{\text{ref}}$ ):

$$f = K_p(x_{\text{ref}} - x) + K_d(\dot{x}_{\text{ref}} - \dot{x}). \quad (2)$$

Inserting equation 2 into 1 the EOM of the feedback-controlled system becomes:

$$m\ddot{x} + (d + K_d)\dot{x} + (k + K_p)x + \alpha x^3 = K_p x_{\text{ref}} + K_d \dot{x}_{\text{ref}}. \quad (3)$$

The simplified CBC exploits the unique parametrization of S-curves, which many nonlinear systems hold to. Varying  $x$ , the S-curves can be traced at constant excitation frequencies. In the closed-loop experiment the displacement is controlled by the reference signal  $x_{\text{ref}}$ . The excitation force settles automatically according to equation 2. Therefore, in an experiment the amplitude of the reference signal is increased while the resulting force is measured and the S-curves are

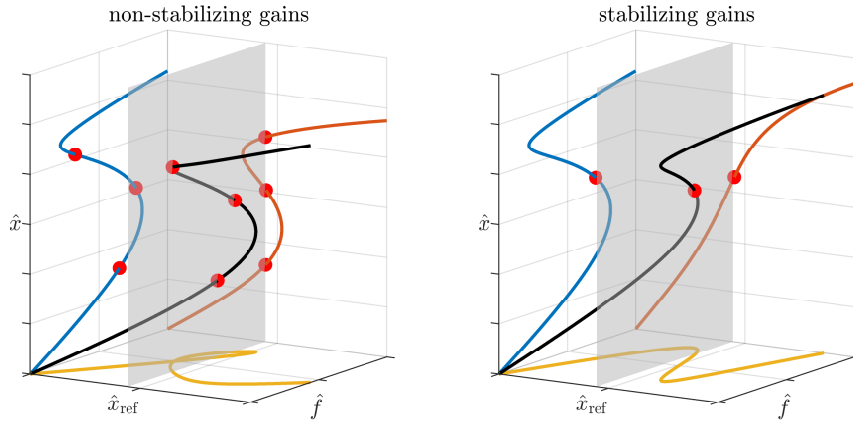


Figure 3: Comparison of the  $\hat{x}(\hat{x}_{\text{ref}})$ -parametrization for a set of stabilizing and non-stabilizing controller gains (at a constant frequency).

reconstructed from the amplitude values of  $x$  and  $f$ . In figure 3, the correlations of the amplitudes  $\hat{x}, \hat{f}$  and  $\hat{x}_{\text{ref}}$  for two sets of controller gains are given as 3-dimensional curves. These curves result from the solution of equation 3 under the assumption of harmonic oscillations (Harmonic Balance Method). The gain settings are chosen for a non-stabilizing effect in the left panel and a stabilizing effect in the right panel. The blue, red and yellow curves are projections into different parameter spaces. The blue curves are the already discussed S-curves. S-curves are exploited to characterize the system and therefore this curves must remain independent of the controller settings. Trying to measure the S-curve with inappropriate controller settings can result in cutting of the extreme points (i.e. the bifurcation points), as shown in section Experimental Validation. The red curves map the reference amplitudes  $\hat{x}_{\text{ref}}$  to corresponding values of  $\hat{x}$ . These shapes are parameterized differently for the two sets of controller gains. For stabilizing control, it is desired that the correlation of  $\hat{x}_{\text{ref}}$  and  $\hat{x}$  becomes unique. This means that for any value of  $\hat{x}_{\text{ref}}$  there should be only one corresponding value of  $\hat{x}$ . This is, what the gray section plane, which runs along a constant value of  $\hat{x}_{\text{ref}}$ , indicates. If there is only a single solution (operation point), oscillation on the unstable branch of the S-curve can be tuned specifying a certain reference amplitude  $\hat{x}_{\text{ref}}$ . If there are multiple intersections, the system will automatically settle to a stable solution. From this theoretical considerations, one can claim that the required constraint for a stabilizing control in CBC is the following: *the control gains are optimally set, when the parameterization of  $\hat{x}$  and  $\hat{x}_{\text{ref}}$  becomes unique.*

### Derivation of Optimal Control Gains

In order to find the desired control settings for the Duffing-oscillator, the corresponding  $\hat{x}_{\text{ref}}(\hat{x})$ -curve is studied analytically. However, the general workflow can be applied to any other nonlinear system, although it may be necessary to extend the principle to a semi-analytical or numerical approach. First, the reference signal is defined to be harmonic and it is assumed that the fundamental harmonic dominates the system response while higher harmonics can be neglected. This approach is known as Harmonic Linearization or Harmonic Balance Method (HBM):

$$\begin{aligned} x &\approx \tilde{x} = \hat{x} \sin(\Omega t), & \dot{\tilde{x}} &= \Omega \hat{x} \cos(\Omega t), & \ddot{\tilde{x}} &= -\Omega^2 \hat{x} \sin(\Omega t) \\ x_{\text{ref}} &= \hat{x}_{\text{ref},s} \sin(\Omega t) + \hat{x}_{\text{ref},c} \cos(\Omega t), & \dot{x}_{\text{ref}} &= \Omega (\hat{x}_{\text{ref},s} \cos(\Omega t) - \hat{x}_{\text{ref},c} \sin(\Omega t)). \end{aligned} \quad (4)$$

The varying phase relation between excitation and response is expressed by splitting the reference signal into sine and cosine components but can also be described by complex numbers, [22]. Next, the nonlinear restoring force is approximated in terms of its Fourier series considering the fundamental harmonic  $\Omega$ :

$$\alpha \tilde{x}^3 = \alpha \hat{x}^3 \sin^3(\Omega t) \approx \frac{a_0}{2} + a_1 \cos(\Omega t) + b_1 \sin(\Omega t), \quad (5)$$

where  $a_0, a_1$  and  $b_1$  are defined as:

$$a_0 = \frac{1}{\pi} \int_{-\pi}^{\pi} f_{\text{nl}} d\varphi, \quad a_1 = \frac{1}{\pi} \int_{-\pi}^{\pi} f_{\text{nl}} \cos(\varphi) d\varphi, \quad b_1 = \frac{1}{\pi} \int_{-\pi}^{\pi} f_{\text{nl}} \sin(\varphi) d\varphi \quad (6)$$

With  $\varphi = \Omega t$ . From eq.6 it follows that in the present example  $a_0 = a_1 = 0$ . Thus, equation 5 turns into:

$$\alpha \hat{x}^3 \sin^3(\Omega t) \approx \alpha \frac{3}{4} \hat{x}^3 \sin(\Omega t). \quad (7)$$

Combing equations 3, 4 and 7 gives:

$$\begin{aligned} &\hat{x} \left( -m\Omega^2 + k + K_p + \alpha \frac{3}{4} \hat{x}^2 \right) \sin(\Omega t) + \hat{x} (d + K_d) \Omega \cos(\Omega t) \\ &= (K_p \hat{x}_{\text{ref},s} - \Omega K_d \hat{x}_{\text{ref},c}) \sin(\Omega t) + (K_p \hat{x}_{\text{ref},c} + \Omega K_d \hat{x}_{\text{ref},s}) \cos(\Omega t). \end{aligned} \quad (8)$$

Because sine and cosine are orthogonal to each other, equation 8 can be further split into terms which contain only sine or cosine components:

$$\begin{aligned}\hat{x}_{\text{ref},c} &= \frac{\Omega}{K_p} ((d + K_d)\hat{x} - K_d\hat{x}_{\text{ref},s}), \\ \hat{x}_{\text{ref},s} &= \frac{\hat{x} (K_d\Omega^2 (d + K_d) + K_p (-m\Omega^2 + k + K_d + \alpha\frac{3}{4}\hat{x}^2))}{K_d^2\Omega^2 + K_p^2}.\end{aligned}\quad (9)$$

It can now be solved for the reference amplitude  $\hat{x}_{\text{ref}}$  and the  $\hat{x}_{\text{ref}}(\hat{x})$ -curve can be derived as a function of the controller gains:

$$\hat{x}_{\text{ref}}(K_p, K_d, \hat{x}) = \sqrt{\hat{x}_{\text{ref},c}^2 + \hat{x}_{\text{ref},s}^2} = \frac{\hat{x} \sqrt{\Omega^2 (d + K_d)^2 + (-m\Omega^2 + k + K_p + \alpha\frac{3}{4}\hat{x}^2)^2}}{\sqrt{K_d^2\Omega^2 + K_p^2}}.\quad (10)$$

Equation 10 is visualized in the left panel of figure 4 for a set of non-stabilizing, critical and stabilizing controller gains. In the right panel of figure 4 the gradient of equation 10 for the same gain settings is given. It is obvious that in order to achieve the desired unique parametrization of  $\hat{x}_{\text{ref}}(\hat{x})$ , the curve must be monotonous. That means the gradient  $\hat{x}'_{\text{ref}}$  must remain positive for all values of  $\hat{x}$ . For critical gains the two extreme points of  $\hat{x}_{\text{ref}}(\hat{x})$  (blue curve) merge into a single saddle point (red curve). Here the  $\hat{x}_{\text{ref}}(\hat{x})$ -curve has a horizontal tangent, which means the gradient has only a single zero point. This is why, for gains above this values the closed-loop system becomes stable.

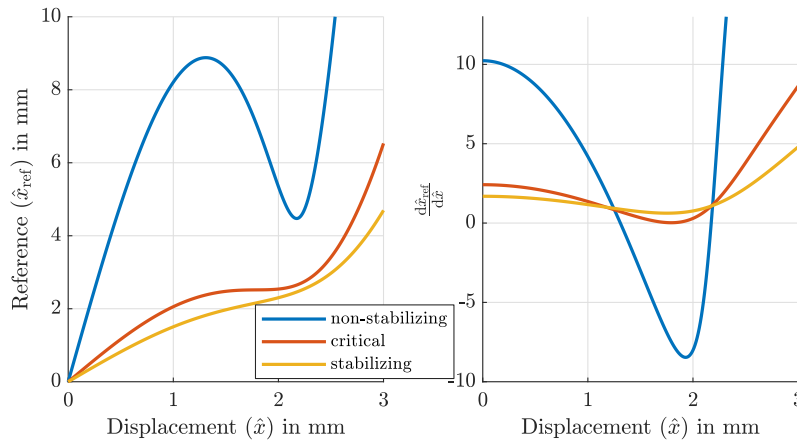


Figure 4: Comparison of the  $\hat{x}_{\text{ref}}(\hat{x})$ -curve for a set of stabilizing and non-stabilizing and critical controller gains (at a constant frequency).

First, the special case of a differential controller ( $K_p = 0$ ) is studied. The D-component is sufficient to stabilize most systems featuring nonlinear stiffness. With a differential controller the derivative of equation 10 can be analytically expressed as:

$$\begin{aligned}\hat{x}'_{\text{ref}} &= \frac{d\hat{x}_{\text{ref}}}{d\hat{x}} = \frac{1}{K_d\Omega} \left( \gamma + \frac{\gamma'}{2\gamma} \right) \\ \text{where } \gamma &= \sqrt{\Omega^2 (d + K_d)^2 + \left( m\Omega^2 - k - \alpha\frac{3}{4}\hat{x}^2 \right)^2} \\ \text{and } \gamma' &= \left( \frac{9}{4}\alpha^2\hat{x}^4 + 3(k - \Omega^2m)\alpha\hat{x}^2 \right)\end{aligned}\quad (11)$$

In order to find the critical value  $K_{d,\text{crit}}$ , the gradient  $\hat{x}'_{\text{ref}}$  is set equal to zero, from which follows:

$$2\gamma^2 + \gamma' = 0.\quad (12)$$

Equation 12 can be rewritten as monic polynomial:

$$\hat{x}^4 + \underbrace{\frac{16}{9\alpha}(k - \Omega^2m)}_p \hat{x}^2 + \underbrace{\frac{16}{27\alpha^2} \left( (d + K_d)^2\Omega^2 + (k - \Omega^2m)^2 \right)}_q = 0.\quad (13)$$

Solutions of equation 13 for  $\hat{x}$  are extreme points of  $\hat{x}_{\text{ref}}(\hat{x})$ . However, the condition for the critical gain is that the extreme points merge into a saddle point, which means that equation 13 will have only one solution. Substituting  $z = \hat{x}^2$

the solution can be expressed as:

$$z = -\frac{p}{2} \pm \sqrt{\frac{1}{4}p^2 - q}. \quad (14)$$

There is only one condition under which equation 14 has zero points at  $z = -\frac{p}{2}$ :

$$\frac{1}{4}p^2 = q. \quad (15)$$

Solving equation 15 leads to the critical gain  $K_{d,crit}$ , which is a function of the oscillation frequency  $\Omega$  and the mass, damping and stiffness coefficients of the system:

$$K_{d,crit} = \pm(k - \Omega^2 m) \frac{1}{\sqrt{3}\Omega} - d \quad (16)$$

Note, that although both solutions (negative and positive) are mathematically correct, only the negative is practically relevant. Equation 16 also reveals that the critical gain is independent of the nonlinear coefficient  $\alpha$ . That means, it is only necessary to determine the structural parameter of the underlying linear system for optimal controller settings. In most cases this can be easily done performing a linear experimental modal analysis at low level oscillations.

The critical proportional gain  $K_{p,crit}$  can be derived in an analogous way, setting  $K_d = 0$  in equation 10. The proportional gain  $K_{p,crit}$  becomes:

$$K_{p,crit} = \pm\sqrt{3}d\Omega + m\Omega^2 - k. \quad (17)$$

Here, again the solution has mathematically a positive and a negative sign. However, the negative solution is the only valid one. Note, that for  $K_p \neq 0$ ,  $K_p$  becomes part of the solution  $z$  in equation 14, which means increasing  $K_p$  also increases the displacement amplitude  $\hat{x}$  where the saddle point occurs. That means, that the proportional gain alters the general shape of the  $\hat{x}_{ref}(\hat{x})$ -parametrization. This fact can be exploited to increase the spatial resolution of the measured curves at some intervals. Although the single proportional-controller has a stabilizing effect in theory, experience shows that in practice this case is rather irrelevant. In real-life applications always a PD-controller should be chosen over a pure P-controller. Without a D-component, the system very slowly approaches a steady state. A PD-controller significantly reduces the settling time.

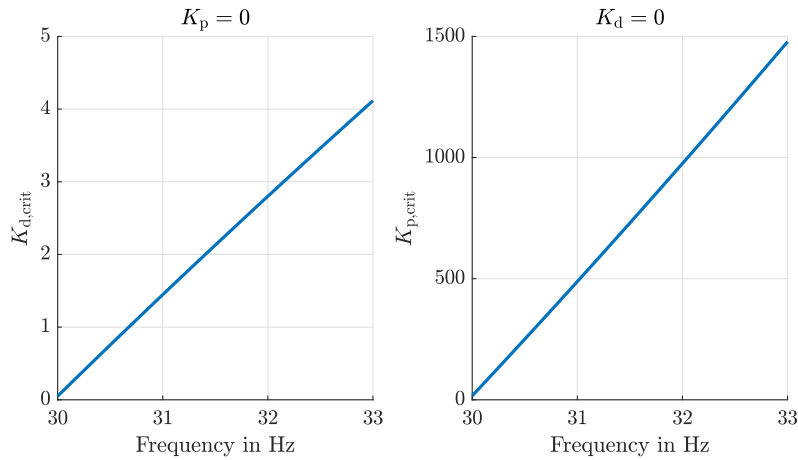


Figure 5: Critical controller gains for different excitation frequencies.

Figure 5 shows the curves corresponding to equations 16 and 17 for the experimental system from section Experimental Validation in the relevant range of frequencies. The linear natural frequency (LNF) of the system is just below 30 Hz. For frequencies higher than this, stabilization is necessary because the NLF has a significant overhang, see figure 1. It can be seen, that the critical gains increase almost linearly with the frequency starting at the LNF. At 31 Hz the displacement became so high that the upper bifurcation point could not be reached with the used displacement sensor. However, from the equations it is evident, that both values continue to grow for higher frequencies.

It can be seen that the critical P-gain is about two orders of magnitude above the critical D-gain. Accordingly, considering a displacement and a velocity signal with the same signal to noise ratio, the measurement noise is amplified many times more by a stabilizing P-controller than by a pure D-controller. Therefore, in a practical implementation it depends on the measured variable and signal quality, whether the D-component or the P-component should be weighted more, as several combinations will equally stabilize the system. If a PD-controller is employed, the critical gains are reduced because both values contribute to stabilization. This can be mathematically derived performing the calculation from equations 11 to 15 for both,  $K_p \neq 0$  and  $K_d \neq 0$ . The critical differential gain  $K_{d,crit}$  is then a function of the proportional gain  $K_p$ :

$$K_{d,crit} = -\frac{1}{\sqrt{3}\Omega} (k + K_p) + \frac{1}{\sqrt{3}} m\Omega - d. \quad (18)$$

$m$	$k$	$d$	$\alpha$
0.1964 kg	6926 $\frac{\text{N}}{\text{m}}$	0.1046 $\frac{\text{Ns}}{\text{m}}$	$5.27 \cdot 10^7 \frac{\text{N}}{\text{m}^3}$

Table 1: Parameter of the Duffing-oscillator.

From equation 18 it can be concluded, that  $K_{d,\text{crit}}$  decreases linearly with  $K_p$  but still increases with  $\Omega$ . Following equation 18 stability maps can be constructed, compare figure 6. Here, the critical gains from equation 16 and 17 are intersections of the curves with the vertical and horizontal axes. The curves themselves are defined by equation 18. These maps are intended to find proper controller gains for different frequencies. Both components can be weighted as preferred by the user. As long as the values lie above the curves, the feedback-control has the desired stabilizing effect on the system.

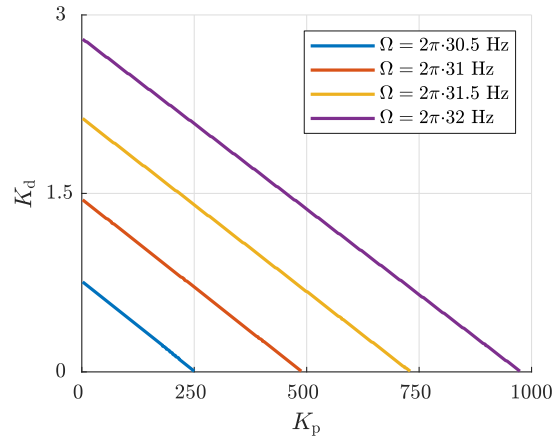


Figure 6: Stability map for the Duffing-oscillator with system parameters from section Experimental Validation. The lines indicate the stability margin for different excitation frequencies.

### Experimental Validation

The theoretical considerations are experimentally validated. Hereby, the focus lies on the hypothesis from equation 10, and the resulting critical controller gains according to figures 5 and 6. The experimental setup is a single-degree-of-freedom oscillator, which has already been investigated in [14] and [23]. Figure 7 shows a picture and a schematic representation of the system. The main components are the fixed frame ①, the voice-coil actuator (VCA) ② and the mass ③. The mass is suspended by guitar strings in the middle of the frame. It is excited by the VCA and moves out of the frame plane as illustrated by the schematic view. The VCA is actuated by a power amplifier for electrodynamic shakers made by TIRA. The amplifier supports a current-mode which enables to control the output current directly. The velocity and displacement of the mass is measured at position ④. Due to the geometric nonlinearity between mass displacement and strain of the guitar strings the oscillator exhibits a significant nonlinear stiffness. Following figure 7 the restoring force can be formulated as:

$$F_k = 8k_s \left( 1 + \frac{l_v - l_g}{\sqrt{l_g^2 + x^2}} \right). \quad (19)$$

Here  $k_s$  is the axial stiffness of the strings,  $l_v$  is the elongation due to the preload force,  $l_g$  is the free length from mass to corner and  $x$  is the displacement. Approximating equation 19 by its truncated Taylor series the nonlinear EOM of the forced system can be written in analogy to equation 1 as:

$$m\ddot{x} + d\dot{x} + \underbrace{8\frac{k_s l_v}{l_g}}_k x + \underbrace{4\frac{k_s(l_g - l_v)}{l_g^3}}_\alpha x^3 = f. \quad (20)$$

It can be seen, that this particular system can be well described by a Duffing-oscillator. In order to find the appropriate model parameters, a two-step procedure was conducted. First, the parameters of the underlying linear system ( $m, d, k$ ) were determined by sweeping through the resonance frequency at a low level excitation (0.02 N from 29 – 31 Hz). The frequency response was observed and the modal parameters were extracted, which already correspond to the physical parameters in the case of a single-degree-of-freedom system. The excitation force was reverse calculated from the measured current flowing through the VCA, because both are proportional. In the second step, the system was excited with a significantly larger force of about 0.1 N. Here during the sweep-up the system showed a jump phenomenon. Assuming the EOM from equation 20 is accurate, the nonlinear coefficient  $\alpha$  was determined by an optimization algorithm based on Newton's

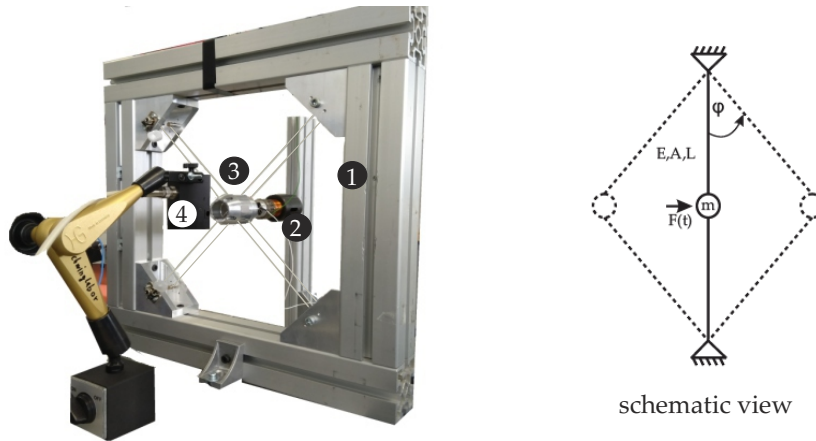


Figure 7: Photograph and schematic view of the Duffing-oscillator.

$\Omega/(2\pi)$	30.3 Hz	30.5 Hz	30.7 Hz
$K_{d,crit}$	0.47	0.75	1.03

Table 2: Theoretical critical differential gains ( $K_p = 0$ ).

method. For this purpose, the measured time-domain data was matched with a time step simulation until the residuum (difference between the envelopes of both signals) became minimal. As an input signal for the time step integration the actually measured force resp. current signal was used. Figure 8 shows a comparison between the measured velocity and the envelope of the model output after optimization. The estimated system parameters are summarized in table 1. In the following the linear part was used to calculate critical gains corresponding to figures 5 and 6. Three different excitation frequencies were chosen to validate the formulas from equation 10, 16 and 18. The critical differential gains  $K_{d,crit}$  for these frequencies are given in table 2.

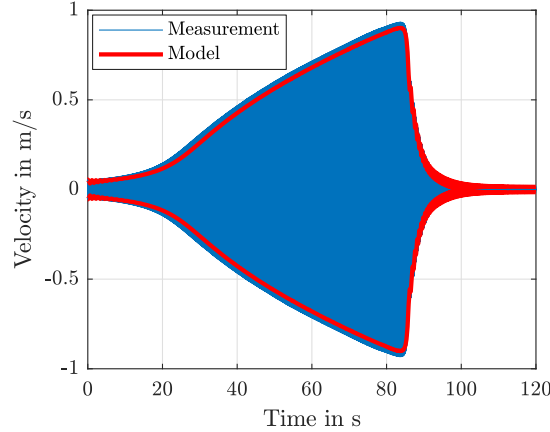


Figure 8: Comparison between measurement and model of the Duffing-oscillator.

After parametric characterization, the CBC procedure was applied to the test-rig. For each CBC run the controller gains were varied around the calculated critical values. The reference amplitude was increased in 0.2 mm steps. First, a pure differential controller was investigated, therefore the P-component was set to zero. In figure 9 the estimated results are shown in comparison with the theoretical curves (black), given by equation 10. On the top panels the  $\hat{x}_{ref}(\hat{x})$ -curves are shown for different settings of controller gains and on the bottom panels the corresponding S-curves are plotted. The blue markers indicate values close to the critical gains, see table 2. The red and green markers represent gains below and above the critical values. All measured curves are in good agreement with the theoretical results. Here, especially the red curves illustrate the negative effect of a poorly chosen controller gain. As those curves are not monotonous, at some point the system suddenly transits from one stable solution branch to the other stable solution branch (from  $\textcircled{A}$  to  $\textcircled{B}$  on the upper graph). Therefore, a whole interval of displacement amplitudes is missing on this measurements and the upper bifurcation point is skipped. Similar results were achieved for all three frequencies. The gains with the blue markers are chosen to be close to the critical values. Here, the bifurcation regions are sampled quite well. Best results are achieved for controller gains 30 – 50 % above the critical values (yellow markers).

The more common case of a PD-controller was also investigated. Therefore,  $K_d$  was set to a constant value and  $K_p$  was

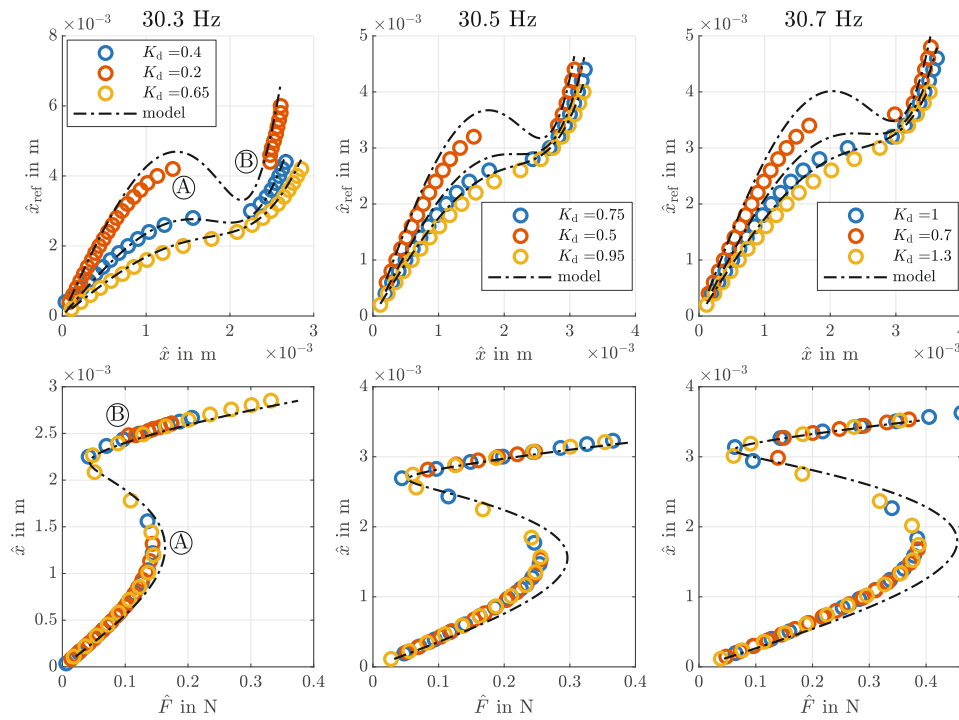


Figure 9: Comparison between measured  $\hat{x}_{\text{ref}}(\hat{x})$ -curves resp. S-curves and theoretical curves. For all curves applies  $K_p = 0$ .

varied. The aim of this experiment was to validate the stability map from figure 6. The results for three different settings of  $K_d$  and totally seven pairs of gain settings are shown in figure 10. The graph on the upper left side shows the distribution of the control gains and the remaining three graphs represent the corresponding S-curves. All curves are captured at 33.3 Hz. The crosses correspond to values close to the theoretical stability margin, which is highlighted as the dotted black line, while circles are values within the instability area. It can be seen, that for all unstable gain settings (circles) the S-curves are not entirely captured. Parts of the unstable branches are skipped. However, for values just above the stability margin the s-curves are sampled well, although  $\hat{x}_{\text{ref}}(\hat{x})$  has been incremented by the same step size in all experiments. For  $K_d = 0.3$  a third measurement was performed, which is represented by the red stars. Here, the proportional gain was chosen significantly higher than in the other two cases. It appears that featuring a higher P-component, the unstable branch is sampled at a finer spatial resolution. This has been predicted in section already. The reason is that the proportional gain shifts the turning point of the  $\hat{x}_{\text{ref}}(\hat{x})$ -curve towards higher amplitudes. As a result the  $\hat{x}_{\text{ref}}(\hat{x})$ -curve is unfolded to a more parabolic shape and so the spacing between two adjacent  $\hat{x}$ -values becomes smaller, as figure 11 illustrates. The marker style and color in figure 11 correspond to those from figure 10. Depending on the controller setting it is possible to trade of between a finer resolution of the lower stable branch or the unstable and upper branch. For either setting the controller is stabilizing. No significant drop of signal quality by the higher proportional gain ( $K_d = 0.3$  and  $K_p = 61$  compared to  $K_d = 0.3$  and  $K_p = 142$ ) was observed. However, measurement noise could be amplified by higher gains and thus decrease signal quality or even lead to instability of the closed loop system. Therefore, controller gains should not be set too high. Critical gains are good starting points for a manual optimization.

To confirm this, a proportional gain of  $K_p = 500$  and a differential gain of  $K_d = 1.5$  for the final analysis of the system dynamics was chosen. According to figure 6 this gain settings are stabilizing up to 32 Hz. As at 30.9 Hz the displacement amplitude corresponding to the upper bifurcation point became to large for the sensor, only S-curves from 29.6 Hz to 30.9 Hz in 0.1 Hz are studied in figure 12. As it can be seen, all S-curves have an excellent spatial resolution of the unstable branch. Note, that these are raw results, no filtering or averaging has been applied to the fundamental Fourier coefficients. The scattered measurement data points (black) have been interpolated by cubic splines. This is represented by the gray manifold, similar to figure 1. The red curves in the upper graph of figure 12 are the contour plots of this manifold at specific forcing amplitudes. These NLFR-curves are shown in the bottom graph in detail. Due to the chosen interpolation type they appear noisy, here a higher frequency resolution would have been beneficial. Nevertheless, the NLFR-curves give a better understanding of the system response near resonance, including two stable and one unstable branch, than a sweep test like in figure 8. Conclusively it can be stated, that the theoretical considerations from section Derivation of Optimal Control Gains, led to an analytical formula for the critical gains and enabled a significant speed up of the CBC measurement compared to previous studies, [14]. The time consuming part of finding stabilizing controller gains by trial and error could be omitted and was replaced by an efficient preliminary analysis of the examined system. The Duffing-oscillator approximation for the investigated single-degree-of-freedom system is in good agreement with measurements in terms of  $\hat{x}_{\text{ref}}(\hat{x})$ - and S-curves.

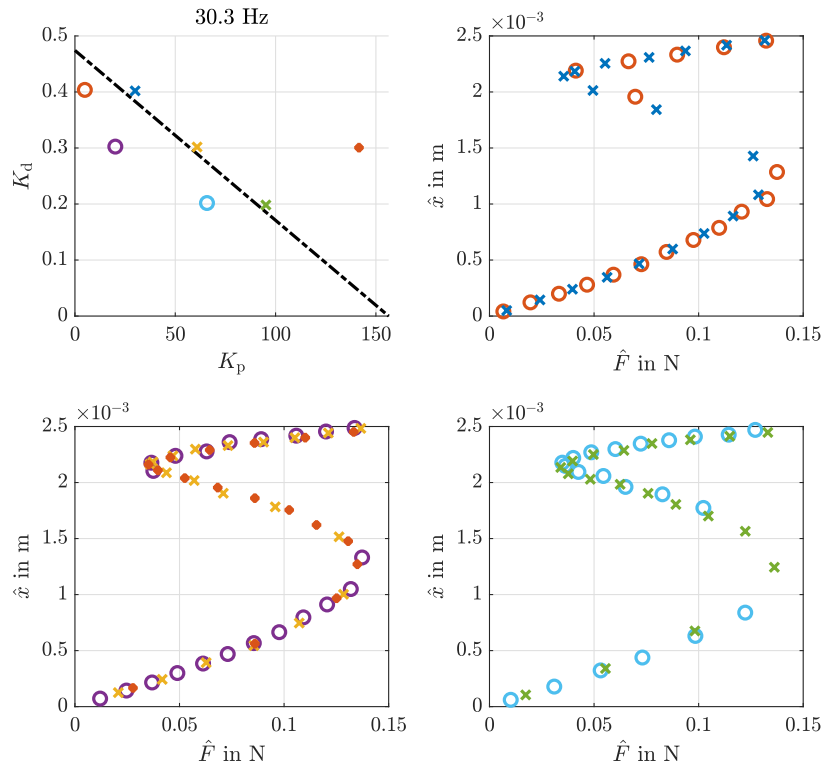


Figure 10: Comparison between controller gains at different locations of the stability map.

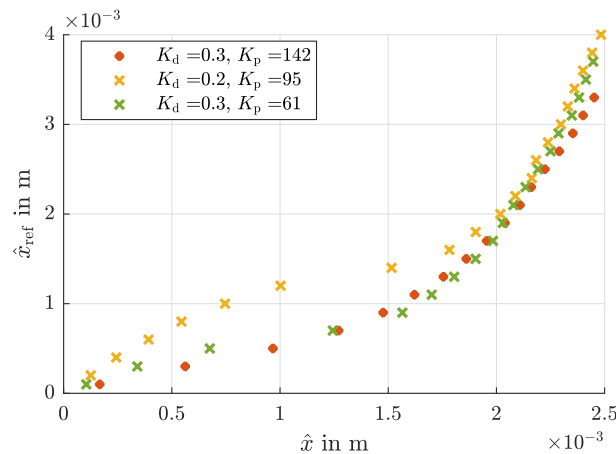


Figure 11: Comparison of different stabilizing controller gains.

## Conclusion

In this paper an analytical formula has been derived to find critical controller gains for the stabilizing control of a Duffing-oscillator exploiting a PD-controller. Critical gains are described as the minimum necessary gains to stabilize the unstable periodic orbits of the system. The main application is intended to be the control based continuation of systems that can be approximated by a Duffing-oscillator model. For the formula the structural parameters of the underlying linear system are needed, which can be extracted from experimental modal analysis at low level excitation. The prefactor of the nonlinear cubic term is not required. Although in this paper the derivation has been conducted and validated for the single-degree-of-freedom Duffing-oscillator only, the workflow can be generalized and applied to any nonlinear system. The process incorporates the following steps:

- Find an approximate model for the nonlinear system
- Include controller rule in the equation of motion
- Apply Harmonic Balance to solve for  $\hat{x}_{\text{ref}}(\hat{x})$
- Investigate  $\hat{x}_{\text{ref}}(\hat{x})$  (or its derivative)
- Critical gains are those values which unfold  $\hat{x}_{\text{ref}}(\hat{x})$  so that the curve becomes unique

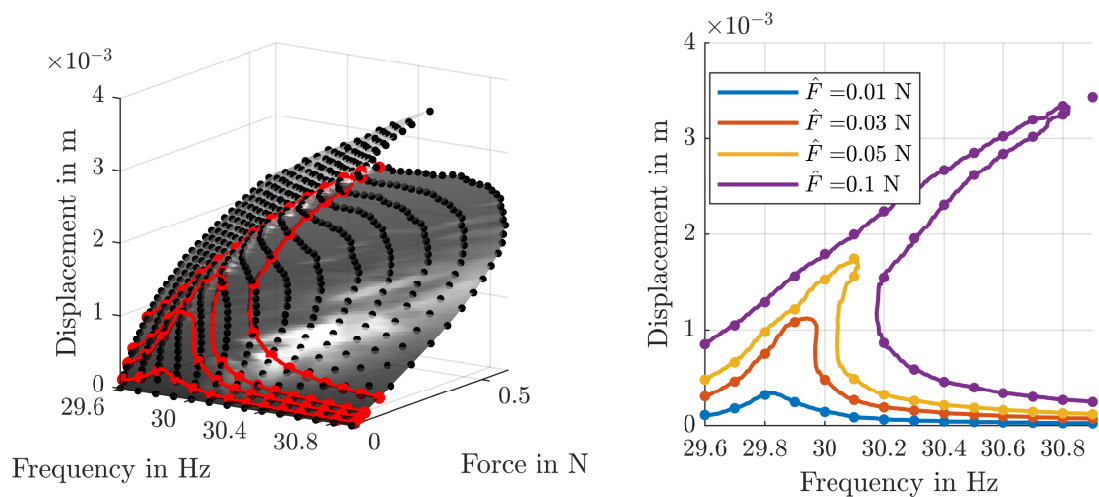


Figure 12: Experimentally determined manifold (left) and reconstructed NLFRC-curves (right).

## References

- [1] A. H. Nayfeh, D. T. Mook, *Nonlinear Oscillations*, John Wiley & Sons, Inc., 1995.
- [2] M. P. Mignolet, A. Przekop, S. A. Rizzi, S. M. Spottswood, A review of indirect/non-intrusive reduced order modeling of nonlinear geometric structures, *Journal of Sound and Vibration* 332 (10) (2013) 2437–2460. doi:10.1016/j.jsv.2012.10.017.
- [3] C. Touze, M. Vidrascu, D. Chappelle, Direct finite element computation of non-linear modal coupling coefficients for reduced-order shell models, *Comput Mech* 54 (2014) 567–580. doi:10.1007/s00466-014-1006-4.
- [4] J. J. Thomsen, *Vibrations and Stability*, 2nd Edition, Springer-Verlag Berlin Heidelberg, 2003.
- [5] J.-P. Noël, G. Kerschen, Nonlinear system identification in structural dynamics: 10 more years of progress, *Mechanical Systems and Signal Processing* 83 (2017) 2–35.
- [6] J. Sieber, B. Krauskopf, Control based bifurcation analysis for experiments, *Nonlinear Dyn* 51 (2008) 365–377. doi:10.1007/s11071-007-9217-2.
- [7] J. Sieber, B. Krauskopf, D. Wagg, S. Neild, A. Gonzalez-Buelga, Control-based continuation of unstable periodic orbits, *Journal of Computational and Nonlinear Dynamics* 6 (1) (2010). doi:10.1115/1.4002101.
- [8] D. Barton, S. Burrow, Numerical continuation in a physical experiment: Investigation of a nonlinear energy harvester, *Journal of Computational and Nonlinear Dynamics* 6 (2011) 011010. doi:10.1115/1.4002380.
- [9] D. Barton, B. Mann, S. Burrow, Control-based continuation for investigating nonlinear experiments, *Journal of Vibration and Control* 18 (4) (2012) 509–520. doi:10.1177/1077546310384004.
- [10] D. Barton, J. Sieber, Systematic experimental exploration of bifurcations with noninvasive control, *Phys. Rev. E* 87 (2013) 052916. doi:10.1103/PhysRevE.87.052916.
- [11] D. Barton, Control-based continuation: Bifurcation and stability analysis for physical experiments, *Mechanical Systems and Signal Processing* 81 (2017) 54–64. doi:10.1016/j.ymsp.2015.12.039.
- [12] L. Renson, A. Shaw, D. Barton, S. Neild, Application of control-based continuation to a nonlinear structure with harmonically coupled modes, *Mechanical Systems and Signal Processing* 120 (2019) 449–464. doi:10.1016/j.ymsp.2018.10.008.
- [13] F. Schilder, E. Bureau, I. F. Santos, J. Thomsen, J. Starke, Experimental bifurcation analysis - continuation for noise-contaminated zero problems, *Journal of Sound and Vibration* 358 (2015) 251–266. doi:10.1016/j.jsv.2015.08.008.
- [14] G. Kleyman, M. Paehr, S. Tatzko, Application of control-based-continuation for characterization of dynamic systems with stiffness and friction nonlinearities, *Mechanics Research Communications* 106 (2020) 103520. doi:10.1016/j.mechrescom.2020.103520.
- [15] L. Renson, A. G. Buelga, D. Barton, S. Neild, Robust identification of backbone curves using control-based continuation, *Journal of Sound and Vibration* 367 (2016). doi:10.1016/j.jsv.2015.12.035.
- [16] L. Renson, D. Barton, S. Neild, Experimental tracking of limit-point bifurcations and backbone curves using control-based continuation, *International Journal of Bifurcation and Chaos* 27 (2017) 1730002. doi:10.1142/S0218127417300026.
- [17] L. Renson, J. Sieber, D. Barton, A. Shaw, S. Neild, Numerical continuation in nonlinear experiments using local gaussian process regression, *Nonlinear Dynamics* 98 (4) (2019) 2811–2826. doi:10.1007/s11071-019-05118-y.
- [18] G. Abeloos, L. Renson, C. Collette, G. Kerschen, Control-based continuation of nonlinear structures using adaptive filtering, in: G. Kerschen, M. Brake, L. Renson (Eds.), *Nonlinear Structures & Systems*, Volume 1. Conference Proceedings of the Society for Experimental Mechanics Series., Springer, Cham, 2020, pp. 109–112. doi:10.1007/978-3-030-47626-7\_17.
- [19] E. Bureau, F. Schilder, M. Elmegård, I. Santos, J. Thomsen, J. Starke, Experimental bifurcation analysis of an impact oscillator – determining stability, *Journal of Sound and Vibration* 333 (21) (2014) 5464–5474. doi:10.1016/j.jsv.2014.05.032.
- [20] E. Bureau, F. Schilder, I. Santos, J. Thomsen, J. Starke, Experimental bifurcation analysis of an impact oscillator: Tuning a non-invasive control scheme, *Journal of Sound and Vibration* 332 (22) (2013) 5883–5897. doi:10.1016/j.jsv.2013.05.033.
- [21] Y. Li, H. Dankowicz, Adaptive control designs for control-based continuation in a class of uncertain discrete-time dynamical systems, *Journal of Vibration and Control* 26 (21-22) (2020) 2092–2109. doi:10.1177/1077546320913377.
- [22] S. Tatzko, M. Jahn, On the use of complex numbers in equations of nonlinear structural dynamics, *Mechanical Systems and Signal Processing* 126 (2019) 626–635. doi:10.1016/j.ymsp.2019.02.041.
- [23] S. Mojrzisch, J. Wallaschek, J. Bremer, An experimental method for the phase controlled frequency response measurement of nonlinear vibration systems, in: *Proc. Appl. Math. Mech.*, Vol. 12, 2012, pp. 253–254. doi:10.1002/pamm.201210117.